Particle impact on a cohesive granular media

V Ralaiarisoa, P. Dupont, Ahmed Ould El Moctar, F. Naaim-Bouvet, L. Oger, A. Valance

Particle impact on a cohesive granular media

V. Ralaiarisoa,[1,2] P. Dupont,[3] A. Ould El Moctar,[4] F. Naaim-Bouvet,[2] L. Oger,[1] and A. Valance[1]

[1] *Univ Rennes, CNRS, Institut de Physique de Rennes, UMR 6251, 35042 Rennes, France*
[2] *Univ. Grenoble Alpes, INRAE, UR ETNA, 38000 Grenoble, France*
[3] *Univ Rennes, INSA Rennes, LGCGM, 35043 Rennes, France*
[4] *Univ. Nantes, CNRS, Laboratoire Thermique et Energie de Nantes, UMR 6607, 44306 Nantes, France*

(Dated: April 15, 2022)

We investigate numerically the impact process of a particle of diameter d and velocity V_i onto a cohesive granular packing made of similar particles via two-dimensional discrete element method simulations. The cohesion is ensured by liquid bridges between neighboring particles and described by short range attraction force based on capillary modeling. The outcome of the impact is analyzed through the production of ejected particles from the packing, referred to as the splash process. We quantify this production as function of the impact velocity for various capillary strength Γ and liquid content Ω. The numerical data indicate that the splash process is modified when the dimensionless cohesion number $Co = 6\Gamma/\rho_p g d^2$ (where ρ_p is the particle density, d its diameter and g the gravitational acceleration) exceeds a critical value of the order of the unity. Above this value, we highlight that the ejection process is triggered above a threshold impact Froude number, $Fr = V_i/\sqrt{gd}$, which depends both on Γ and Ω and scales as $\Gamma^\beta \Omega^\delta$, where the values of the exponents are found close to 1/2 and 1/6, respectively, and can be derived from rational physical arguments. Importantly, we show that above the threshold, the number of splashed particles follows a linear law with the impact Froude number as in the cohesionless case.

I. INTRODUCTION

The process of impact of a particle onto a granular bed is an important issue in various physical and geophysical systems. Wind blown sand and saltation transport is an emblematic example where the impact process plays a relevant and important role [1–4]. Saltation is the primary mode of particle transport in wind blown sand. It consists of successive hops along the surface. Saltating grains are propelled by the wind and rebound on the sand bed. As they are highly energetic, they are able to eject particles from the sand bed. The understanding of the impact process, also termed splash, is a key ingredient to model correctly aeolian sand transport. A large number of studies including wind tunnel experiments [5, 6], computer simulations [7–9], and model collision experiments consisting in propelling a single particle [10–14], were devoted to the splash process. These studies provide a rather complete picture of the splash process in the context of non-cohesive granular beds.

The influence of the bed cohesion on the splash process has received very little attention although this issue is crucial in the context of aeolian transport with moist sand [15] or snow [16]. We investigate here the role of the granular bed cohesion on the splash process through numerical simulations in using discrete element method (DEM) [17]. We consider granular packings where inter-particle cohesion is ensured by capillary bridges and investigate the result of the impact of an incident particle for various cohesion strength.

The article is organized as follows. Section 2 describes the numerical set-up and the force model used in the DEM simulation. The numerical method is first validated on cohesionless granular packings (Section 3) and then applied to the case of cohesive packings (Section 4). Discussion and conclusion are presented in Section 5.

II. NUMERICAL METHOD AND SIMULATION SET-UP

We have conducted two-dimensional simulations of the impact of a particle onto a cohesive granular packing using discrete element method (DEM) [17]. The principle of DEM simulations is to treat each grain as a sphere (of diameter d and mass s) subject to gravity and contact forces with the other grains.

Interaction model is performed by using a combination of a linear visco-elastic and Coulomb modeling. Two grains i and j interact when overlapping, such as $\delta_{ij} = r_{ij} - (d_i + d_j)/2 < 0$, with r_{ij} the center-to-center grains separation. The force applied by grain i on grain j is split into a normal and tangential component, $F_n^{i\to j}$ and $F_t^{i\to j}$, respectively. The normal contact force is modeled using a spring dash-pot model,

$$F_n^{i\to j} = \begin{cases} -(k_n \delta_{ij} + \gamma_n \dot{\delta_{ij}}) & \text{for } \delta_{ij} < 0 \\ 0 & \text{for } \delta_{ij} > 0 \end{cases} \quad (1)$$

where k_n and γ_n are the spring stiffness and the damping coefficient, respectively, while the tangential contact force is described by a regularized Coulomb friction model [17, 18],

$$F_t^{i\to j} = -\min(|\gamma_t v_t|, |\mu F_n^{i\to j}|) \quad (2)$$

where γ_t is the tangential damping coefficient, v_t is the tangential component of the relative velocity and μ is the friction coefficient.

In addition to contact forces, we add an inter-particle cohesive force that mimics the force produced by a liquid meniscus. The so-called capillary force is modeled

following the same approach as used in [19–21]:

$$F_c^{i\to j} = \begin{cases} F_c^{max} & \text{for} \quad \delta_{ij} < 0 \\ F_c^{max}\left(1 - 1/\sqrt{1+\frac{V_l}{\pi d\delta_{ij}^2}}\right) & \text{for} \quad 0 < \delta_{ij} < \xi \\ 0 & \text{for} \quad \delta_{ij} > \xi \end{cases} \tag{3}$$

where V_l is the volume of the liquid bridge and ξ is the critical rupture distance. At contact (i.e.,$\delta_{ij} = 0$), the magnitude of the capillary force is maximum and is given by:

$$F_c^{max} = \pi d\Gamma \cos\theta \,, \tag{4}$$

where Γ is the surface tension and θ the contact angle. When the particles get apart (i.e. $\delta_{ij} > 0$), the capillary force decreases with increasing δ_{ij}. Beyond $\delta_{ij} = \xi$ the liquid bridge breaks apart and the capillary force vanishes. The rupture distance, in the limit of perfect wetting (i.e., $\theta = 0$), is taken to be as [22]:

$$\xi = V_l^{1/3} \tag{5}$$

where V_l is the volume of the liquid bridge.

The key physical variables governing the capillary force are the grain diameter, the surface tension Γ and the volume of the liquid bridges. This leads us to introduce two non-dimensional numbers: (i) a cohesion number Co defined as the ratio of the maximum capillary force F_c^{max} to the gravitational force F_g,

$$Co = \frac{F_c^{max}}{F_g} = \frac{6\Gamma}{\rho_p d^2 g} \,, \tag{6}$$

where ρ_p is the particle density and g the gravitational acceleration, and (ii) the water content Ω defined as the ratio of the total liquid mass to the total solid mass,

$$\Omega = \frac{(N_l/2)\rho_l V_l}{(\pi/6)\rho_p d^3} \tag{7}$$

where N_l is the mean number of liquid bridges connected to a particle and ρ_l is the liquid density. We assume here that all the capillary bridges have the same volume V_l. In addition, a capillary bridge forms when two particles are in contact such as N_l is equal to the mean number of contacts of a given particle [28]. In a 3D disordered packing, the mean number of contact is 6 while in a 2D packing, it is 4. The determination of this value from our 2D simulations gives us a value very close to 4. In the following, we will thus set $N_l = 4$.

Equations of motion for each particle are calculated by applying Newton second law and a Velocity-Verlet scheme is used for the time integration with a time step dt. Table I displays the values of the parameters used in the simulations for the contact and capillary forces.

Simulations require several steps. We first create a 2D non-cohesive granular packing by filling a square box of dimensions $40d \times 40d$. The packing is built using a pluviation method with non-cohesive particles (see Fig. 1).

TABLE I: DEM parameters

Parameter	Value
Contact force	
k_n	$2.10^5 - 2.10^7$ (mg/d)
e_n	0.88
μ	0.5
γ_n/γ_t	1
dt	$10^{-4} - 10^{-5}(\sqrt{d/g})$
Cohesion force	
Co	$0 - 1000$
Ω	$0 - 10\%$

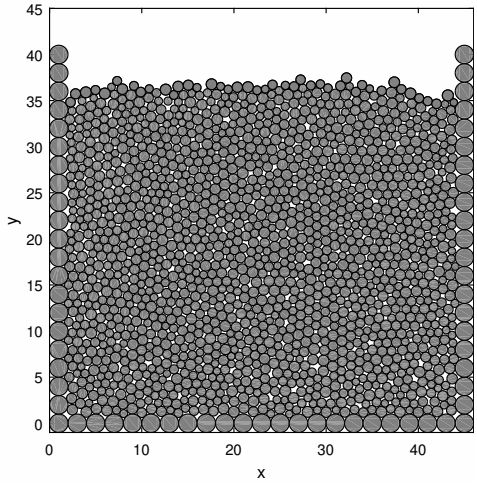

FIG. 1: 2D packing built with 16000 particles of mean diameter d using pluviation method in a square box with dimensions $40d \times 40d$. To avoid crystallization, the particles of the packing have a polydispersity of 20% and the walls of the box consist of spherical particles of diameter $2d$. The mean volume fraction of the packing is $\phi = 0.8$.

To avoid crystallization, the grains of the packing have a mean diameter d with a size dispersion of 20% and the side and bottom walls of the box are made of spherical particles of diameter $2d$. Once the packing relaxes to its equilibrium, we implement the cohesive forces for the particles that are in contact. The introduction of capillary forces induces a micro-rearrangement of the particles of the packing. Once the cohesive packing has reached its new mechanical equilibrium, we can proceed with the collision process. A particle is propelled on the packing with a given incident speed V_i and angle θ_i and the result of the impact is analyzed through the rebound and the splashed particles. In order to get reasonable statistics of the splash process, the collision is repeated about 50 times by changing the impact location in a random manner in the vicinity of the center of the packing.

Importantly, we checked that the system is large enough in order that the shock wave created by the impact is dissipated through the packing before reaching

the boundaries. We indeed run a few simulations with a larger system (i.e., $80d \times 80d$) and the latter produced similar results.

III. VALIDATION OF THE NUMERICAL MODEL WITH A NON-COHESIVE PACKING

To validate our numerical model, we first performed simulations with a non-cohesive granular packing. The outcomes of these simulations are compared to the experimental results from Beladjine et al. [13]. The collision process is analyzed both through the rebound of the incident bead and the resulting ejected particles. For convenience, we introduce a dimensionless impact velocity defined as $V_i/\sqrt{gd}$ and referred to as the impact Froude number Fr. The incident angle θ_i is defined as the angle between the impact velocity and the horizontal.

A. Rebound

The rebound of the incident bead is usually characterized through the restitution coefficient e defined as the ratio between the rebound and impact velocity. Figure 2a presents the evolution of the averaged restitution coefficient $\bar{e}$ with impact angle θ_i for various impact velocities ranging from $20\sqrt{gd}$ and $80\sqrt{gd}$. We also plotted the averaged vertical restitution coefficient $\overline{e_z}$ defined as the ratio of the vertical rebound velocity to the vertical impact velocity (see Fig. 2b). Both restitution coefficients decreases with increasing impact angle and are independent of the impact velocity. These results follow the same trends as the experimental outcomes reported in [13]. In addition to this qualitative agreement, we obtain a remarkable quantitative agreement. Our numerical results are remarkably approximated by the empirical laws proposed by Beladjine et al. [13]:

$$\bar{e}(\theta_i) = A - B\sin\theta_i\,, \tag{8}$$

$$\bar{e_z}(\theta_i) = \frac{A_z}{\sin\theta_i} - B_z\,, \tag{9}$$

where A, B, A_z and B_z are fitting parameters. The best fit to our numerical data provides similar values as those found in [13]: $A \approx 0.87$, $B \approx 0.72$, $A_z \approx 0.30$ et $B_z \approx 0.15$. Note that in order to satisfy $e = e_z$ for normal impact, A, B, A_z and B_z are linked by the following relation: $A - B = A_z - B_z$.

B. Ejected particles

The other important feature of the splash process concerns the ejected particles and their production according to the impact velocity and incident angle. We define an ejected particle as a particle which reaches a vertical position greater than a particle diameter above the bed surface as done in previous works [13, 14]. In other words, the vertical velocity of ejection should be greater than $\sqrt{2gd}$. Fig. 3 presents the average number of ejected particles as a function of the impact velocity for several angles of incidence ranging from 10° to 90°. The number of ejected particles increases with increasing impact speed and this trend can be captured by a linear law similar to the one proposed in [13]:

$$\bar{N}_{ej} = N_0(\theta_i)(Fr - Fr_c) \tag{10}$$

where $Fr = V_i/\sqrt{gd}$ is the dimensionless impact velocity also referred as to the impact Froude number. N_0 and Fr_c are fitting parameters. N_0 is found to depend on the incident angle θ_i while Fr_c is independent of the impact angle θ_i and can be interpreted as the critical Froude number above which particles are ejected from the packing. The linear fits to our data give us a critical Froude number $Fr_c = 12$ and indicate that N_0 is proportional to the fraction of energy of the incident particle transferred

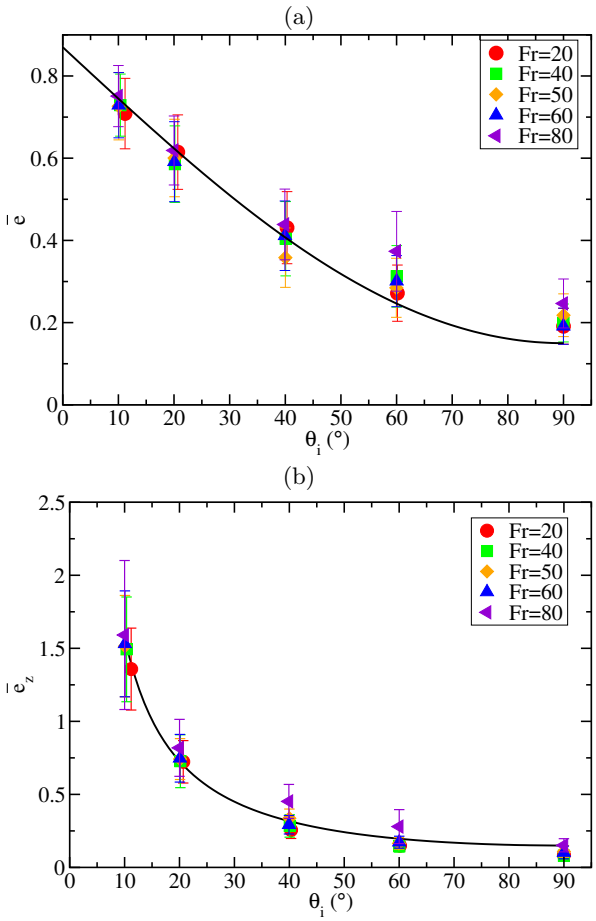

FIG. 2: Variation of the restitution coefficients $\bar{e}$ (a) and $\bar{e_z}$ (b) as a function of the incident angle θ_i for different Froude number $Fr = V_i/\sqrt{gd}$ ranging from 20 to 80. The solid lines represent empirical laws proposed by Beladjine et al. [13].

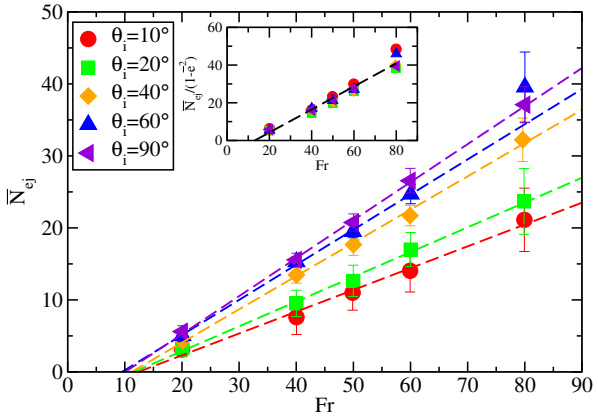

FIG. 3: Variation of the mean number of ejected particles $\bar{N}_{ej}$ as a function of the impact Froude number $Fr = V_i/\sqrt{gd}$ for various incident angles θ_i ranging from 10° to 90°. The dash lines represent linear fits to the data using Eq. 10. Inset: Mean number of ejected particles renormalized by the fraction of energy of the incident bead transferred to the packing (i.e., $\bar{N}_{ej}/(1-\bar{e}^2)$) as a function of the Froude number Fr. The dash line represents the best linear fit to our data.

to the packing (i.e.,$(1-\bar{e}^2)$):

$$N_0(\theta_i) \approx \alpha \left(1 - \bar{e}^2(\theta_i)\right) \qquad (11)$$

where α is a numerical constant ($\alpha \approx 0.61$). The variation of N_0 with the incident angle is in agreement with the experimental findings reported in [13]. However, we observe quantitative differences. Beladjine et al. [13] found a higher critical Froude number and a smaller value for α (i.e., $Fr_c = 40$ and $\alpha = 0.32$). Our numerical model thus overestimates the number of ejected particles in comparison with the experimental results in [13]. This difference can be ascribed to the two-dimensional configuration of the numerical simulations. The energy of impact is expected to be dissipated more efficiently in a 3D packing than in a 2D one. This results from the higher coordination number of a 3D arrangement and the possibility for the energy to dissipate through a greater number of paths. As the production of ejected particles is closely related to the dissipation process, it is expected to be enhanced in the case of a 2D packing.

As a summary, the numerical simulations reproduce faithfully the main features of the splash process in the context of non-cohesive granular packing and can be thus employed with confidence to investigate the influence of the cohesion on the splash process.

IV. SPLASH PROCESS WITH A COHESIVE PACKING

A. Construction of cohesive packings

We return here to the numerical process employed for building cohesive packings. We recall that we start from a 2D non-cohesive packing built by pluviation. We then set the capillary forces and wait for the packing to relax towards its new mechanical equilibrium. We choose a large enough dimensionless stiffness $K = k_n/\Gamma$ (i.e., $K \geq 5.10^3$) such that the particle packing remains homogeneous and with the same volume fraction as in the cohesionless case (see Appendix for further discussion).

B. Influence of the Cohesion number

We now investigate the influence of the packing cohesion on the splash process. We focus first on the effect of the strength of the capillary force by varying the cohesion number but keeping the water content fixed and equal to $\Omega_0 = 1\%$. We carried out 7 series of numerical collision experiments corresponding to different cohesion number ranging from 0.1 to 10^3. For each value of the cohesion number, the incident speed was varied between 20 to $120\sqrt{gd}$ keeping the incident angle fixed ($\theta_i = 10°$). We also vary the incident angle from 10° to 60° keeping the impact velocity constant.

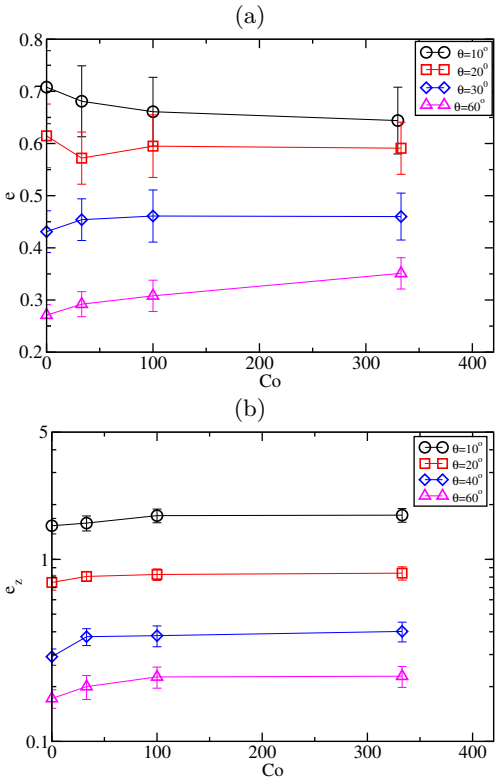

FIG. 4: Variation of the restitution coefficients $\bar{e}$ et $\bar{e_z}$ as a function of the cohesion number for various incident angles. The impact Froude number and the water content are set to $Fr = 60$ and $\Omega = 1\%$.

The numerical results show that the rebound of the impacting particle exhibits to first order the same features as those for a non-cohesive packing, in the range of

cohesion number investigated so far. More precisely, the restitution coefficients $\bar{e}$ et $\bar{e}_z$ present only weak changes when the cohesive strength is varied (see Figure 4). $\bar{e}_z$ increases weakly but systematically with increasing Co. $\bar{e}$ shows contrasting variation according to the impact angle. For grazing impact, $\bar{e}$ decreases with increasing cohesion strength while for greater impact angle we observe the reverse trend. The variations remain however weak in comparison with those induced by change of the impact angle.

In contrast, the cohesion of the packing has a major effect on the ejected particles when the cohesion number goes well beyond 1 (see Fig. 5). For $Co \geq 10$, the critical Froude number required to trigger particle ejection is changed and increases with increasing cohesion strength. Despite of this, the number of ejected particles still presents a linear increase with increasing incident speed, as in the non-cohesive case,

$$\bar{N}_{ej} = N_0(Co)\ [Fr - Fr_c(Co)] \tag{12}$$

but with altered values of the critical Froude number Fr_c and of the coefficient N_0. Fr_c increases with increasing cohesion number while N_0 decreases. Both variations act together in the same direction and lead to a decrease of the mean number of ejected particles when the cohesion is increased.

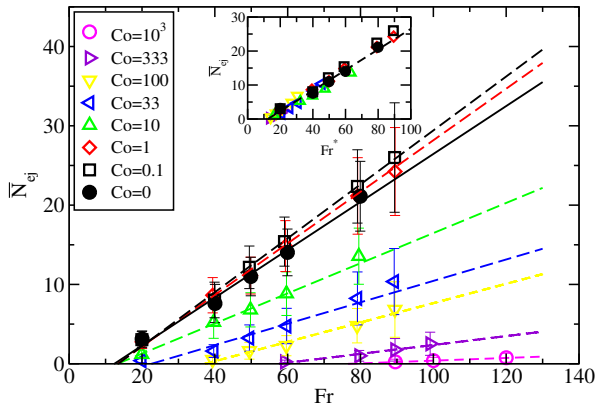

FIG. 5: Mean number of ejected particles $\bar{N}_{ej}$ as a function of the Froude number Fr for various values of the cohesion number Co. The incident angle is kept constant and equal to $\theta_i = 10^\circ$ and $\Omega = 1\%$. Inset: Mean number of ejected particles $\bar{N}_{ej}$ as a function of the modified Froude number Fr^* (cf. Eq. 15).

Fig. 6 displays the variation of the critical Froude number Fr_c and N_0 as a function of the cohesion number. The critical Froude number Fr_c is unchanged ($Fr_c \approx 12$) as long as the cohesion umber remains below a critical value $Co_c \approx 5$. Beyond this value, Fr_c increases with increasing Co according to a power law,

$$Fr_c = Fr_c^{(0)} \left(\frac{Co}{Co_c}\right)^{\beta_1}, \tag{13}$$

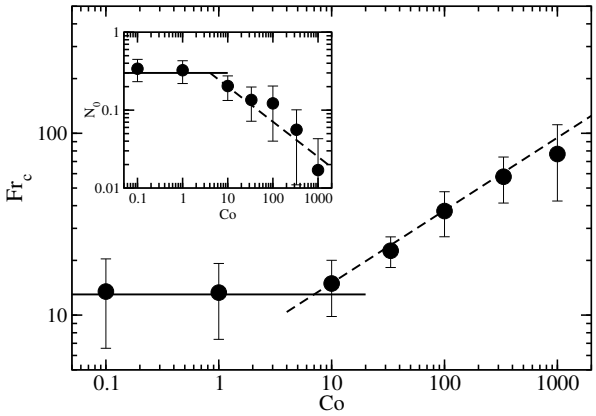

FIG. 6: Variation of critical Froude number Fr_c and the slope N_0 (see Inset) as a function of the cohesion number. The horizontal solid lines represent the non-cohesive limit where the dashed lines stand for the best fits using the following scaling laws: $Fr \propto Co^{\beta_1}$ et $N_0 \propto Co^{-\beta_2}$ with $\beta_1 \approx 0.4$ and $\beta_2 \approx 0.45$.

where $Fr_c^{(0)}$ is the critical Froude number for a cohesionless packing and the scaling law exponent is $\beta_1 \approx 0.4$. Similarly, the coefficient N_0 is constant up to the critical value Co_c. Then it decreases with increasing Co according to the following power law (see inset of Fig. 6),

$$N_0 = N_0^{(0)} \left(\frac{Co}{Co_c}\right)^{-\beta_2}, \tag{14}$$

with $\beta_2 \approx 0.45$. $N^{(0)}$ refers to the value obtained for a non-cohesive packing. The exponents β_1 and β_2 of the scaling laws are surprisingly similar and are not far from the value of 1/2. In the rest of the article, we will take $\beta_1 \approx \beta_2 \equiv \beta \approx 2/5$.

On the basis of the above results, it may be useful to introduce a modified Froude number Fr^*:

$$Fr^* = \left(\frac{Co}{Co_c}\right)^{\beta} Fr \tag{15}$$

where $Co_c \approx 5$. With this, the law for the number of ejected particles can be recast into the simple expression:

$$\bar{N}_{ej} = N_0^{(0)}(Fr^* - Fr_c^{(0)}) \tag{16}$$

with $N_0^{(0)}(\theta_i = 10^\circ) \approx 0.3$ and $Fr_c^{(0)} \approx 12$. The inset of Fig. 5 displays the variation of the number of ejected particles as a function of the modified Froude number Fr^*. The data collapse on the master curve given by Eq. 16.

The above numerical outcomes were obtained for a given impact angle $\theta_i = 10^\circ$. We now vary the impact angle from $\theta_i = 10^\circ$ to 60°. The inset of Fig 7 illustrates the variation of the number of ejected particles as a function of the Froude number Fr for various impact angles and cohesion number. The effect of the impact angle on

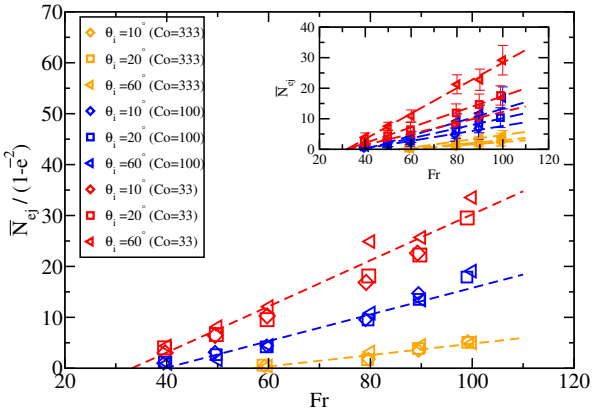

FIG. 7: Variation of the mean number of ejected particles rescaled by $(1-\bar{e}^2)$ as a function of the Froude number Fr for various impact angle θ_i and various cohesion number Co. Inset: Variation of the mean number of ejected particles as a function of the Froude number Fr.

the number of ejected particles is similar as in the non-cohesive case. For a given cohesion number, the mean number of ejected particles increases with increasing angle and this increase is directly linked to the fraction of energy transferred to the packing (i.e., $(1-\bar{e}^2)$) as in the non-cohesive case. Fig. 7 shows that when the mean number of ejected particles is rescaled by $(1-\bar{e}^2)$, the data obtained for different impact angles but similar cohesion strength collapse on an unique linear trend. Thus the law for the mean number of ejected particles and its dependence with the Froude number, incident angle and cohesion number can be cast into the simple following form:

$$\bar{N}_{ej} = N_0^{(0)}(\theta_i)\left(Fr^* - Fr_c^{(0)}\right) \tag{17}$$

with

$$N_0^{(0)}(\theta_i) \approx 0.61\left[1-\bar{e}^{(0)^2}(\theta_i)\right] \tag{18}$$

$$Fr_c^{(0)} \approx 12 \tag{19}$$

Fr^* is the modified Froude number given by Eq. 15. We recall that the superscript (0) refers to quantities obtained in the non-cohesive case. This relationship is a generalization of the law proposed by [13] to cohesive packings. The last step is to investigate the dependence of the Splash process on the water content Ω.

C. Influence of the water content

In the previous section, we studied the effect of capillary force on the Splash process by varying the cohesion number and setting the water content to a constant value $\Omega = 1\%$. We showed that there is a critical value of Co_c above which the Splash process is modified by the cohesion of the packing. We now wish to study the influence of the water content Ω. The value Ω is tuned by changing the amount of the liquid in the packing through the volume of the liquid bridge V_l. We recall that in our modeling the water content has only an influence on the critical distance required to break up the liquid bridge but does not modified the maximum cohesion strength.

To do this, we vary the water content from 0 to 10% and keep fixed the cohesion number and the incident angle which are set to 100 and 10°, respectively. Fig. 8

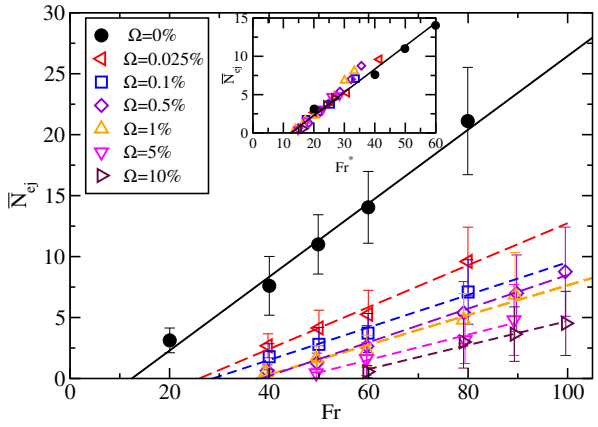

FIG. 8: Mean number of ejected particles $\bar{N}_{ej}$ as a function of the Froude number Fr for various water content ranging from 0% to 10%. $\theta_i = 10°$ and $Co = 100$. Dash lines stand for the best fit to the data with linear laws. Inset: Mean number of ejected particles as a function of the modified Froude number Fr^*.

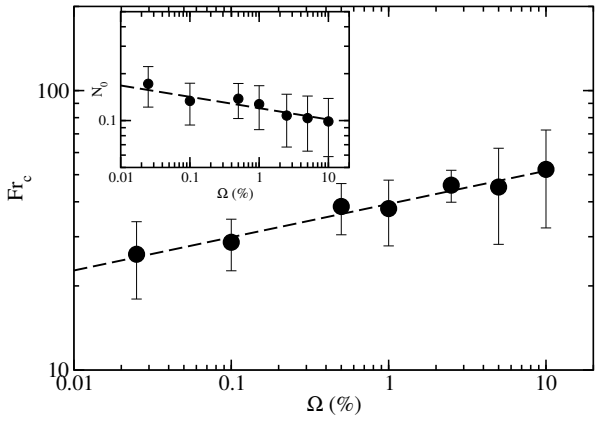

FIG. 9: Variation of the critical Froude number Fr_c and coefficient N_0 (inset) as function of the water content Ω.

depicts the variation of the mean number of ejected particles as a function of the Froude number for various water content. First, the critical Froude number Fr_c above which particles are ejected increases with increasing water content. Second, above the critical Froude number, the data still show a linear trend with a slope which decreases with increasing water content. As a result, for a

given Froude number, the mean number of ejected particles decreases with increasing water content, as expected.

The variation of the critical Froude number Fr_c and the slope N_0 with Ω are well captured by power laws (see Fig. 9):

$$Fr_c = Fr_c^{(0)} \left(\frac{\Omega}{\Omega_c}\right)^{\delta_1} \quad \text{for } \Omega > \Omega_c \tag{20}$$

$$N_0 = N_0^{(0)} \left(\frac{\Omega}{\Omega_c}\right)^{-\delta_2} \quad \text{for } \Omega > \Omega_c \tag{21}$$

with $\delta_1 \approx 0.125$, $\delta_2 \approx 0.11$ and $\Omega_c \approx 10^{-4}$. Further comments follow. Ω_c is the critical value above which the features of the ejection process are altered by the cohesion. This value is expected to depend on the cohesion number as we shall see in the next subsection. Similarly as for the dependence on the cohesion number, we find that the scaling exponents δ_1 and δ_2 are close to each other. We will therefore set $\delta_1 \approx \delta_2 \equiv \delta \approx 1/8$. We also note that the influence of the water content on the splash process is much weaker than that of the cohesion number. We indeed have a scaling law with an exponent δ which is relatively modest compared to the exponent β ($\beta \approx 2/5$).

D. Crossed influence of the cohesion number and water content

In view of the results found on the number of ejected particles and its dependence on the cohesion number and the water content, it may be tempting to combine the two scaling laws established in the previous section. Doing so, this leads to conjecture that the critical Froude number Fr_c and the coefficient N_0 should obey the following laws:

$$Fr_c = Fr_c^{(0)} \left(\frac{Co}{Co_{c_0}}\right)^{\beta} \left(\frac{\Omega}{\Omega_0}\right)^{\delta} \quad \text{for } Co > Co_c(\Omega) \tag{22}$$

and

$$N_0 = N_0^{(0)} \left(\frac{Co}{Co_{c_0}}\right)^{-\beta} \left(\frac{\Omega}{\Omega_0}\right)^{-\delta} \quad \text{for } Co > Co_c(\Omega) \tag{23}$$

where $Co_c(\Omega)$ is the critical value of the cohesion number above which the splash process is altered by the cohesion for a given water content Ω and is given by:

$$Co_c(\Omega) \approx Co_{c_0} \left(\frac{\Omega}{\Omega_0}\right)^{-\delta/\beta} \tag{24}$$

where $Co_{c_0} \approx 5$ is the critical value for $\Omega_0 = 1\%$ and $\delta/\beta \approx 5/16 \approx 0.3$. This conjecture allows to conciliate the results obtained previously but must be verified for arbitrary values of Ω and Co.

If the above scaling laws hold, we can thus write an explicit law predicting the mean number of ejected particles taking into account the dependence on the Froude number, the incident angle, the cohesion number and the water content:

$$\bar{N}_{ej} = N_0^{(0)}(\theta_i)\left(Fr^* - Fr_c^{(0)}\right) \tag{25}$$

where Fr^* is the modified Froude number given by

$$Fr^* = Fr \left(\frac{Co}{Co_{c_0}}\right)^{\beta} \left(\frac{\Omega}{\Omega_0}\right)^{\delta} \quad \text{for } Co > Co_c(\Omega) \tag{26}$$

where $\beta \approx 2/5$, $\delta \approx 1/8$, and $Co_c(\Omega) \approx Co_{c_0}(\Omega/\Omega_0)^{-\delta/\beta}$ (with $\Omega_0 = 1\%$ and $Co_{c_0} \approx 5$).

To validate this law, we carried out additional simulations of the splash process with a new set of parameters (Co, Ω) not tested before: $Co = 10$ and $\Omega = 5\%$. The incident angle was set to $\theta_i = 10°$. The outcomes are presented in Fig. 10 and are in agreement with the prediction given by Eq. 25. This confirms that the scaling laws we conjectured is relevant.

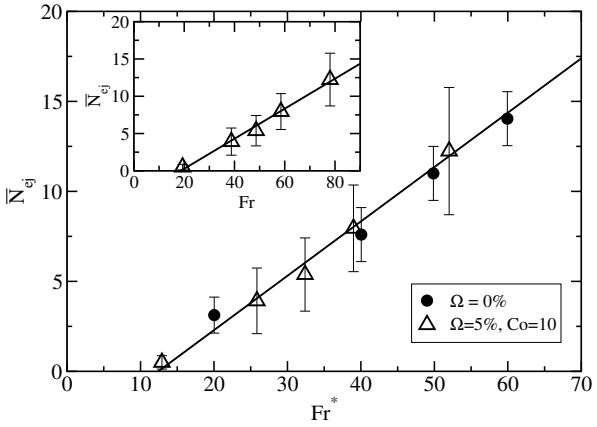

FIG. 10: Variation of the mean number of ejected particles as a function of the modified Froude number Fr^* for $Co = 10$ and $\Omega = 5\%$ (The impact angle is kept fixed: $\theta_i = 10°$). The solid line stands for Eq. 25. Inset: Mean number of ejected particles as a function of the Froude number Fr. The solid line presents a linear fit to the data: $\bar{N}_{ej} = N_0(Fr - Fr_c)$ with $Fr_c \approx 20$ and $N_0 \approx 0.2$.

V. DISCUSSION AND CONCLUSION

2D Numerical simulations of the splash process reveals that there exists a critical cohesion number that depends on the water content above which the splash process is altered by the cohesion. Above this threshold, the cohesion of the packing leads to an increase of the critical Froude number together with a significant decrease of the number of ejected particles. In contrast, no significant effect is observed on the rebound law. Importantly, we were able to establish a law for the number of ejected particles which takes into account the the cohesion strength

and the water content. The law can be written as:

$$\bar{N}_{ej} = N_0(Co, \Omega, \theta_i)\Big\{ Fr - Fr_c\,(Co, \Omega)\Big\} \qquad (27)$$

where the critical Froude number Fr_c and the parameter N_0 depend on Co and Ω, and are given for $Co > Co_c(\Omega)$ by

$$Fr_c = Fr_c^{(0)}\ \left(\frac{Co}{Co_{c_0}}\right)^{2/5}\ \left(\frac{\Omega}{\Omega_0}\right)^{1/8} \qquad (28)$$

and

$$N_0 \approx 0.61\ (1 - e^{(0)^2})\ \left(\frac{Co}{Co_{c_0}}\right)^{-2/5}\ \left(\frac{\Omega}{\Omega_0}\right)^{-1/8} \qquad (29)$$

where $Co_c(\Omega)$ reads

$$Co_c(\Omega) \approx Co_{c_0}\ \left(\frac{\Omega}{\Omega_0}\right)^{-5/16} \qquad (30)$$

and $Co_{c_0} \approx 5$ is the critical value for $\Omega_0 = 1\%$. For $Co < Co_c(\Omega)$, the ejection process is unchanged and $N_0 = N_0^{(0)}$ and $Fr_c = Fr_c^{(0)}$.

Some of these results can be explained by using simple physical arguments. In particular, the exponents of the scaling law for the critical Froude number and critical cohesion number can be derived from energetic considerations. The idea is to estimate the minimum impact energy E_c necessary to trigger the splash process, that is to eject at least one particle from the bed. The outcomes of the splash process with cohesionless packing tell us that this minimum impact energy is: $E_c^{(0)} = mgd\,Fr_c^{(0)}$. Now, in presence of cohesive bonds within the packing, we expect the minimum impact energy to be enhanced by a amount corresponding to the energy necessary to break the liquid bonds of the particle to be ejected from the bed as: $E_c = E_c^{(0)} + E_c^{(1)}$ with $E_c^{(1)} = n\xi\Gamma d = n\xi Co/2d$ (we recall that ξ is the critical size of the liquid bridge above which it breaks down). $E_c^{(1)}$ corresponds to the work required to break n liquid bonds. For a particle at the surface of the packing, n is expected to be between 2 and 4. Consequently, we can infer from this minimum energy a critical Froude number in the case of cohesive packings:

$$Fr_c = Fr_c^{(0)}\sqrt{1 + \frac{n\xi}{2d}Co} = Fr_c^{(0)}\sqrt{1 + nCo\left(\frac{\pi\rho_p\Omega}{12\rho_l}\right)^{1/3}}, \qquad (31)$$

where we used $\xi \approx V_l^{1/3} \approx \left(\pi\rho_p d^3\Omega/12\rho_l\right)^{1/3}$ (see Eqs 5 and 7). The above relationship indicates that the critical Froude number is expected to be altered by cohesion when $Co > 2nd/\xi$ which yields a critical cohesion number:

$$Co_c \approx \left(\frac{2}{n}\right)\left(\frac{\pi\rho_p\Omega}{12\rho_l}\right)^{-1/3} \approx 1.2\,\Omega^{-1/3}\,. \qquad (32)$$

ρ_p and ρ_l were set to 2500 kg/m^3 and 1000 kg/m^3 as in the numerical simulation whereas n was set to 2. This prediction is very close to that obtained in the simulation outcomes (see Eq. 30). The scaling exponent was $-5/16$ which is fairly similar as $-1/3$.

Interestingly, Eq. 31 provides also a prediction of the critical Froude number in the limit of strong cohesion (i.e., $Co \gg Co_c$) which yields

$$Fr_c \propto \Omega^{\delta_p} Co^{\beta_p}\,, \qquad (33)$$

where the predicted scaling exponents are $\delta_p = 1/6$ and $\beta_p = 1/2$. Again, this prediction is in excellent agreement with the numerical outcomes where the scaling exponents were 1/8 and 2/5.

This phenomenological modeling is expected to remain valid in the context of the 3D packings so we strongly believe that these scalings should also hold for 3D cohesive packings. This should however be confirmed by 3D discrete simulations which is currently under investigation.

To conclude, we provided a detailed description of the splash process in case of cohesive packings whose cohesion is ensured by capillary bridge. This set of results could be useful to better understand aeolian transport in the context of moist sand. The new splash laws we propose and in particular Eq. 27 can be a priori easily incorporated into models used to describe aeolian sand transport [23–26]. Indeed, the features of the rebound and of the ejected particles are needed to derive relevant boundary conditions at the bed. For example in [26] a two-phase continuum theory was developed that explicitly incorporates low-velocity moments of the splash function in a calculation of the boundary conditions that apply at the bed. These calculations although lengthy and fastidious can be updated using the generalized equation 27 for the number of the ejected particles which incorporate the influence of the cohesion through the parameters N_0 and Fr_c. This should provide us with mass transport laws in the context of cohesive granular beds.

We believe that these results could be relevant for natural cohesive beds like moist sand. The range of the cohesion strength investigated so far corresponds to typical cohesion level that can be measured for moist sand. According to [27] the cohesion strength of unsaturated sand composed $0.25\,mm$ grain size can reach cohesion number Co of the order of $10 - 100$ when the water content Ω approaches a few percent. Our outcomes predict a significant change of the splash function when the cohesion strength goes beyond 5. So we expect to observe a change of the sand transport properties for moist sand in natural conditions.

Finally, the versatility of the DEM simulations allows to investigate other types of cohesive interactions such as solid bridges which is relevant in the context of snow for example.

Appendix A: Effect of the particle stiffness on the packing of a cohesive bed

We discuss here on the effect of the introduction of cohesive forces on the packing structure according to the stiffness of the particles compared with the strength of the capillary force. Fig 11 shows the evolution of the packing volume fraction as a function of the dimensionless stiffness $K = k_n/\Gamma$ for a given capillary strength Γ. The numerical results indicate that when K is large enough (i.e., $K \gtrsim 5.10^3$), the introduction of the capillary forces does not alter the particle volume fraction of the packing which is identical to that of a cohesionless packing (i.e., $\phi = 0.802$). As the numerical method consider soft particles with a given stiffness k_n, strong cohesion forces could lead to a compression of the packing. On the contrary, if K is decreased below 5.10^3, the volume fraction of the packing increases by a measurable amount. This increase reflects the compressibility of the packing and causes a structural change within the packing, as illustrated in Fig. 12. Dense clusters separated by void appear and the packing does not present any more a homogeneous structure. In the remaining of the paper, we will always consider configurations where the cohesive packing keeps a uniform structure with a volume fraction similar to that of a non-cohesive packing. For this, we make sure that K always remains above 5.10^3. Accordingly, for strong cohesion strength, we increase the stiffness of the particles so that K is above the critical value of 5.10^3.

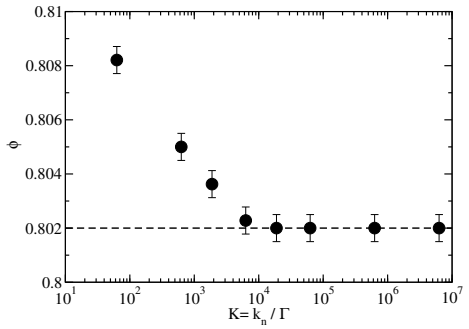

FIG. 11: Particle volume fraction ϕ of a cohesive granular packing as a function of the dimensionless stiffness parameter $K = k_n/\Gamma$. The dashed line represents the particle volume fraction of a non-cohesive packing.

[1] R. A. Bagnold, Methuen, New York (1941).
[2] O. Duran, P. Claudin, and A. Andreotti, Aoelian Research **3**, 243 (2011).
[3] J. Kok, E. Partel, T. Michael, and D. Bou Karam, Report on progress in Physics **75**, 106901 (2012).
[4] A. Valance, K. R. Rasmussen, A. Ould El Moctar, and P. Dupont, Comptes Rendus Physique **16**, 105 (2015).
[5] B. B. Willetts and M. A. Rice, Earth Surface Processes and Landforms **14**, 719 (1989).
[6] M. A. Rice, B. B. Willetts, and I. K. McEwan, Sedimentology **43, 1**, 21 (1996).
[7] B. T. Werner and P. K. Haff, Sedimentology **35**, 189 (1988).
[8] R. S. Anderson and P. K. Haff, Acta Mechanic Supply, 1 , 21 (1991).
[9] L. Oger, M. Ammi, A. Valance, and D. Beladjine, The European Physical Journal E **17**, 467 (2005).
[10] S. Mitha, M. Q. Tran, B. T. Werner, and P. K. Haff, Acta Mechanica **63**, 267 (1986).
[11] B. T. Werner, Journal of Geology **98**, 1 (1990).
[12] F. Rioual, A. Valance, and D. Bideau, Physical Review E. **62**, 2450 (2000).
[13] D. Beladjine, M. Ammi, L. Oger, and A. Valance, Physical Review E. **75**, 061305 (2007).
[14] M. Ammi, L. Oger, D. Beladjine, and A. Valance, Phys. Rev. E **79**, 021305 (2009).
[15] S. L. Namikas and D. J. Sherman, "A review of the effects of surface moisture content on aeolian sand transport," in *Desert Aeolian Processes*, edited by V. P. Tchakerian (Springer Netherlands, Dordrecht, 1995) pp. 269–293.
[16] F. Comola, J. Gaume, J. F. Kok, and M. Lehning, Geophysical Research Letters **46**, 5566 (2019).
[17] P. A. Cundall and O. D. L. Strack, Gotechnique **29**, 47 (1979).
[18] J. Shäfer, S. Dippel, and D. E. Wolf, J. Phys. I France **6**, 5 (1996).
[19] H.-J. Butt and M. Kappl, Advances in Colloid and Interface Science **146**, 48 (2009).
[20] D. Maugis, Journal of Adhesion Science and Technology **1**, 105 (1987).
[21] O. Pitois, P. Moucheront, and X. Chateau, Journal of Colloid and Interface Science **231**, 26 (2000).
[22] G. Lian, C. Thornton, and M. J. Adams, Journal of Colloid and Interface Science **161**, 138 (1993).
[23] G. Sauermann, K. Kroy, and H. J. Herrmann, Physical Review E. **64**, 031305 (2001).
[24] M. Creyssels, P. Dupont, A. Ould El Moctar, A. Valance, I. Cantat, J. T. Jenkins, J. Pasini, and K. Rasmussen, Journal of Fluid Mechanics **625**, 47 (2009).
[25] J. T. Jenkins, I. Cantat, and A. Valance, Physical Review E **82**, 020301R (2010).
[26] J. Jenkins and A. Valance, Physics of Fluid **26**, 073301

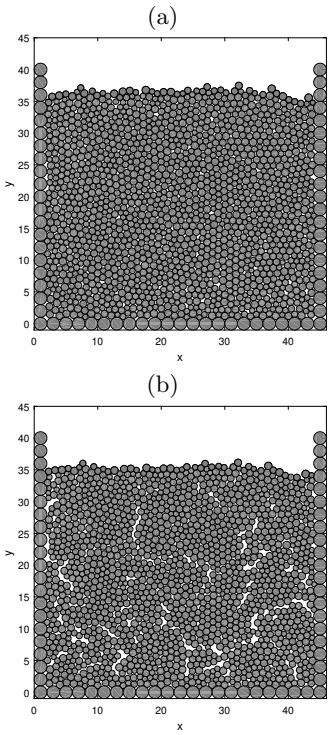

FIG. 12: Illustration of 2D packing cohesive packings with different dimensionless stiffnesses $K = k_n/\Gamma$: (a) $K = 6250$ and (b) $K = 62.5$. When K is decreased below a critical value (i.e., $K \lesssim 5\ 10^3$), strong heterogeneities appear within the bed.

(2014).

[27] V. Richefeu, M. S. El Youssoufi, and F. Radjaï, Phys. Rev. E **73**, 051304 (2006).

[28] Actually, it is not required that two particles be in contact in order that a capillary bridge forms at the thermodynamic equilibrium. The condition is that the inter-particle distance is smaller than $2\,r_k$, where r_k is the so-called Kelvin radius defined by $r_k = \Gamma/(\rho_l k_B T \ln(P_{sat}/P_V))$. r_k is on the order of a few nanometers such as it sets to zero.